# Performance Evaluation of an Integrated Open-Path Eddy Covariance System in a Cold Desert Environment

WEI WANG,[a,b] JIAPING XU,[a] YUNQIU GAO,[a] IVAN BOGOEV,[c] JIAN CUI,[a] LICHEN DENG,[a] CHENG HU,[a] CHENG LIU,[a] SHOUDONG LIU,[a] JING SHEN,[a] XIAOMIN SUN,[d] WEI XIAO,[a] GUOFU YUAN,[d] AND XUHUI LEE[a,e]

[a] *Yale–NUIST Center on Atmospheric Environment, Nanjing University of Information Science and Technology, Nanjing, China*
[b] *Collaborative Innovation Center of Atmospheric Environment and Equipment Technology, Nanjing University of Information Science and Technology, Nanjing, China*
[c] *Research and Development, Campbell Scientific, Inc., Logan, Utah*
[d] *Key Laboratory of Ecosystem Network Observation and Modeling, Institute of Geographic Sciences and Natural Resources Research, Chinese Academy of Sciences, Beijing, China*
[e] *School of Forestry and Environmental Studies, Yale University, New Haven, Connecticut*

(Manuscript received 11 July 2015, in final form 29 July 2016)

ABSTRACT

Performance evaluation of an integrated eddy covariance (EC) instrument called the IRGASON, with a separated EC for reference, was conducted in a desert riparian *Populus euphratica* stand in the lower Tarim River basin in northwestern China. The separated EC consisted of an open-path gas analyzer and a sonic anemometer separated by 20 cm. The IRGASON integrates an open-path gas analyzer and a sonic anemometer into the same sensing volume, thus eliminating sensor separation in comparison to the traditional open-path EC setup. Integrating the infrared gas analyzer's sensing head into the sensing volume of the sonic anemometer had negligible effects on wind speed and friction velocity observations of the IRGASON. Physiologically unreasonable daytime $CO_2$ uptake was observed by both systems during the cold winter season (mean air temperature of −6.7°C), when the trees were dormant without any photosynthetic activities. The mean midday $CO_2$ flux was −1.65 and −1.61 $\mu$mol m$^{-2}$ s$^{-1}$ for the IRGASON and the separated EC setup, respectively. No evidence was found for sensor self-heating as the cause of the apparent uptake $CO_2$ flux. Instead, the uptake $CO_2$ flux appeared to be an artifact of the spectroscopic effect of the IRGASON's gas analyzer. After adjusting for this spectroscopic effect using a relationship with the sensible heat flux, the wintertime IRGASON $CO_2$ flux became physiologically reasonable (mean value of −0.04 $\mu$mol m$^{-2}$ s$^{-1}$).

## 1. Introduction

Since the 1990s, open-path eddy covariance (EC) has been used to measure momentum, heat, water vapor, and trace gas exchanges between the biosphere and the atmosphere across a diverse range of climates and ecotypes (Baldocchi 2014). The traditional open-path EC system, consisting of an open-path infrared gas analyzer (IRGA) and a separate sonic anemometer, suffers from problems of spatial separation, temporal asynchronicity, and sensor self-heating (Bogoev 2014). Being separated by some distance from one another, the two sensors do not measure the same small eddy motion, and the resulting fluxes are systematically underestimated. Post–field frequency response corrections are needed to compensate for the flux loss due to sensor separation (Moore 1986). Temporal asynchronicity, or variable time lag between vertical wind and the gas density of interest, depends on wind speed and wind direction. Open-path EC systems often register physiologically unreasonable $CO_2$ uptake signals under conditions where photosynthesis is not expected (Ham and

Supplemental information related to this paper is available at the Journals Online website: http://dx.doi.org/10.1175/JTECH-D-15-0149.s1.

*Corresponding author address*: Dr. Xuhui Lee, Sara Shallenberger Brown Professor of Meteorology, School of Forestry and Environmental Studies, Yale University, Kroon Hall, 195 Prospect Street, New Haven, CT 06511.
E-mail: xuhui.lee@yale.edu

DOI: 10.1175/JTECH-D-15-0149.1

Heilman 2003) or during the off-season in extremely cold environments (Grelle and Burba 2007) (Table 1). These erroneous results are thought to arise from differences between ambient air temperature and temperature of the measured air volume due to additional heat generated by the instrument electronics or by the loading of solar radiation on the sensor head (Burba et al. 2008).

The sensor self-heating problem associated with separated open-path EC is known to reduce the estimate accuracy of the net ecosystem $CO_2$ exchange. The problem is thought to arise from the Webb–Pearman–Leuning (WPL) density correction algorithm of Webb et al. (1980), which uses the sonic temperature fluctuations measured outside the IRGA optical path. By measuring temperature in the optical path with fine-wire thermometers, Grelle and Burba (2007) found that the traditional WPL correction using sonic-derived sensible heat flux underestimates $CO_2$ efflux by $0.28\,\mu mol\,m^{-2}\,s^{-1}$ (66%) when external heating was applied to their open-path IRGA (model LI-7500, LI-COR Inc.) during the end of growing season. To address the issue, Burba et al. (2008) proposed a theoretical calculation of the additional sensible heat flux and developed a semi-empirical model to correct self-heating during post–data processing for LI-7500. However, no method exists for self-heating correction that can be applied universally to all types of IRGA configurations. Self-heating correction seems to improve the estimation of the carbon budget of terrestrial ecosystems and to reduce the $CO_2$ flux discrepancy between open-path and closed-path EC systems (Grelle and Burba 2007; Burba et al. 2008; Blanken et al. 2009; Järvi et al. 2009; Reverter et al. 2011; Järvi et al. 2012). But not all field data support the practice of post–field self-heating correction. For a temperate mountain grassland in Austria, self-heating correction changes regression statistics only slightly between open- and closed-path EC $CO_2$ fluxes, even when the data during low air temperature were selected (Haslwanter et al. 2009). For a desert ecosystem, applying such correction results in a $CO_2$ flux overestimation of $0.61\,\mu mol\,m^{-2}\,s^{-1}$ in comparison to a closed-path EC, and changes the desert ecosystem to a net $CO_2$ release of 157 and $161\,g\,C\,m^{-2}\,yr^{-1}$ for 2005 and 2006, respectively (Wohlfahrt et al. 2008). The good $CO_2$ flux agreement between open- and closed-path analyzers without self-heating correction was observed by Bowling et al. (2010). Therefore, there is still uncertainty in the importance and necessity of self-heating correction.

Another solution to the self-heating problem is to integrate the IRGA optical path into the sonic anemometer's measuring volume. Given the uncertainties related to post–field corrections, such a hardware solution is very attractive. With the two sensors being directly collocated, any self-heating temperature fluctuations, generated either by the IRGA internal electronics or by solar radiation loading on the sensing head, will be measured by sonic thermometry. The integrated EC system should in principle produce a biologically correct $CO_2$ flux after the WPL correction. One such integrated open-path EC system, called the IRGASON (Campbell Scientific, Inc.), is now available commercially. The IRGASON fully combines the IRGA with a sonic anemometer into a single unit, simultaneously measuring the $CO_2$ and the $H_2O$ density, three-dimensional wind speeds, and temperature in the same air volume. Sensor self-heating is reduced through low power consumption (5 W at 25°C), small diameter (1.9 cm) of the sensing head, and aerodynamic housing (Campbell Scientific, Inc. 2016). The electronic components that consume power and generate heat are confined in a small enclosure 3 m away from the sensing volume, further reducing the interference of artificial heating on the measurement.

Besides the self-heating effect, open-path IRGAs suffer from the spectroscopic effects (e.g., absorption line broadening) that need to be corrected with observations of temperature, pressure, and diluent gas (e.g., $H_2O$) concentration during flux calculation (Detto et al. 2011; McDermitt et al. 2011). A gas analyzer measures the $CO_2$ density in the atmosphere on the basis of infrared light absorption according to the Beer–Lambert law (Welles and McDermitt 2005). The light intensity attenuation in the optical path mainly depends on the $CO_2$ concentration. The $CO_2$ absorption line shape (e.g., half-width) and population distribution (e.g., strength) are affected by barometric pressure, air temperature, and diluent gases mainly from the pressure (collision) broadening mechanism in the atmosphere (Welles and McDermitt 2005; LI-COR, Inc. 2010). These so-called spectroscopic effects should be accounted for by measuring barometric pressure, air temperature, and water vapor concentration in the sensing path. With respect to a closed-path gas analyzer, low-frequency temperature measurements are sufficient to account for such spectroscopic effects. In the case of an open-path gas analyzer, high-frequency temperature fluctuations in the optical path must be measured to fully account for the spectroscopic effect. Currently, single-path, dual-wavelength, nondispersive infrared gas analyzers use a band broadening coefficient or onboard slow-response air temperature measurements to correct the spectroscopic effect. The spectroscopic cross sensitivity arising from direct absorption interference by water vapor and from the pressure broadening effect is generally corrected by

TABLE 1. A summary of the $CO_2$ flux observed with open-path eddy covariance during the off-season or cold winter periods.

| Period | Landscape | Max ($\mu$mol m$^{-2}$ s$^{-1}$) | Mean ($\mu$mol m$^{-2}$ s$^{-1}$) | $T_a$ (°C) | Instrument | Reference |
|---|---|---|---|---|---|---|
| 19–20 Feb 2005 | Burned boreal forest | −5 | | −12 | CSAT3 + LI-7500 | Amiro et al. 2006; Amiro 2010 |
| 9–10 Jan 2005 | | −4.2 | | −23 | CSAT3 + LI-7500 | Amiro et al. 2006 |
| Jan 2003 | Temperature larch forest | −3 | | −5 | TR-61C + LI-7500 | Hirata et al. 2007 |
| Jan 2002–Dec 2004 | Boreal evergreen forest | −3 | | −20 | CSAT3 + LI-7500 | Welp et al. 2007 |
| Jan 2002–Dec 2004 | Boreal deciduous forest | −2 | | −20 | CSAT3 + LI-7500 | Welp et al. 2007 |
| 27 days in late winter, 2004 | Low arctic tundra | −0.9 | | −10 | Gill R3-50 + LI-7500 | Lafleur and Humphreys 2008 |
| 9–11 Apr 2003 | Drained paddy field | −5.9 | | 12 | SAT + LI-7500 | Ono et al. 2008 |
| Winter, 2005–07 | Mojave Desert | | −0.3 (daily) | −2 | CSAT3 + LI-7500 | Wohlfahrt et al. 2008 |
| Oct–Dec 2006 | Beech forest | −2 | | 0 to 12 | Gill R2 + LI-7500 | Järvi et al. 2009 |
| Jan 2007 | Mediterranean alpine shrubland | −2 | | 3 | Metek USA-1 + LI-7500 | Reverter et al. 2010 |
| Winter, 2006–08 | Eucalyptus plantation | −10 | −5 (daily) | 15 to 25 | CSAT3 + LI-7500 | Cabral et al. 2011 |
| 1 Nov 2007–31 Jan 2008 | Arctic polyn'ya | −27.95 | −4.88 (whole period) | −7.5 to −25 | Gill WindMaster Pro + LI-7500 | Else et al. 2011 |
| Winter, 2003–09 | Alpine meadow | −6 | | 0 to −10 | Gill R3 + LI-7500 | Marcolla et al. 2011 |
| 1 Jan–1 Jun 2004 | Sea ice | −14 | −0.7 (daily) | 0 to −35 | CSAT3 + LI-7500 | Miller et al. 2011 |
| Winter, 2006–10 | Urban area | −5 | | −10 | Metek USA-1 + LI-7500 | Järvi et al. 2012 |
| May–Oct 2008 | Subarctic tundra | −4 | −0.48 (daily) | −3.5 | Gill R3 + LI-7500 | Marushchak et al. 2013 |
| Jan 2005–11 | Sea kelp beds | −8 | −4.6 (daily) | 11 | CSAT3 + LI-7500 | Ikawa and Oechel (2015) |
| Winter, 2008–12 | Blanket bog | | −0.5 (daily) | −3 | CSAT3 + LI-7500 | Lund et al. 2015 |

the manufacturer-determined coefficients (e.g., 1.15 for LI-7500A). However, Edson et al. (2011) suggested that these default correction coefficients are problematic for evaluating extremely small $CO_2$ flux and fluctuations in low-flux conditions. Kondo et al. (2014) also showed that the correction coefficient for the direct absorption interference is not optimized to derive the accurate $CO_2$ flux, and that the correction coefficient for the pressure broadening causes $CO_2$ flux overestimation in the same direction as the water vapor flux. Inadequate spectroscopic correction by slow-response air temperature measurement is hypothesized to partly contribute to the ecologically unreasonable $CO_2$ uptake phenomenon with IRGASON (Bogoev et al. 2015). Bogoev et al. (2015) found that the air temperature–related spectroscopic effect can be corrected by using fast air temperature (such as sonic temperature), resulting in much improved agreement in the $CO_2$ flux between an open- and a closed-path EC system.

In this study, we report the results of a performance evaluation of an IRGASON system in a desert environment. The experiment was carried out in a *Populus euphratica* stand in the lower Tarim River basin between the Taklimakan Desert and the Kuluk Desert during a winter (from 16 December 2013 to 3 January 2014) and an early spring (from 12 March to 13 April 2014). In the first period, because the trees were dormant and the temperature was low (mean air temperature of −6.7°C), the natural $CO_2$ flux should be negligibly small, providing an ideal situation for qualifying the self-heating effect and the spectroscopic correction on the $CO_2$ flux measurement. Another objective of the present study is to evaluate the quality of momentum and sensible heat fluxes measured by the integrated system. It is possible that the IRGA sensing head in the sonic measurement volume may interfere with sonic velocity measurement. Another potential drawback of such an integrated open-path EC is that the quality of sensible heat flux measurement may be compromised if IRGA's self-heating is indeed significant. To our best knowledge, this study is the first one evaluating the performance of an integrated open-path EC in a cold desert environment.

## 2. Material and methods

### a. Study site

The field evaluation was conducted in a desert riparian *Populus euphratica* stand (40°25′59″N, 88°01′34″E) in the lower Tarim River basin, between the Taklimakan Desert and the Kuluk Desert, in Xinjiang Province, China (Fig. 1). The site is relatively flat and with an altitude of 844 m. A distinctive feature of the study area is


FIG. 1. (top left) Map showing the location of the desert riparian *Populus euphratica* stand (yellow pin) in the lower Tarim River basin between the Taklimakan Desert and the Kuluk Desert. (bottom left and right) Photographs showing the instrument arrangement.

its cold arid desert (BWk) climate according to the Köppen–Geiger climate classification (Peel et al. 2007). According to meteorological records of the nearby Ruoqiang weather station, the climatological (1981–2010) annual precipitation was 37 mm, which is much less than the annual potential evapotranspiration (2000 mm; Chen et al. 2006). Precipitation generally occurs from June to August, and is scarcely observed in other months. The climatological annual mean air temperature was 12°C. The prevailing wind was from the northeast and the northwest, with an average speed of 2.4 m $s^{-1}$. For our field campaigns, the mean air temperature was −6.7° and 14.1°C in the winter and spring experiments, respectively. The mean water vapor mixing ratio was 2730 and 3390 ppm in the winter and spring experiments, respectively. The mean solar radiation was 91.1 and 195.0 W $m^{-2}$ in the winter and spring experiments, respectively, with corresponding albedo values of 0.28 and 0.27. There was no precipitation during our winter and spring field campaigns.

*Populus euphratica* was the only species in the study area, which stretched along the Tarim River for about 1.5 km, with a width of about 500 m. The average canopy height was 10 m and the canopy closure rate was 0.49. The leaf area index was 0.57 in the peak growing season (Yuan et al. 2015). The winter and early spring experimental periods of this study occurred in the dormant season (from late October to late March of the following year) and in the flowering stage (from the end of March to mid-April) of the *Populus* trees, respectively (Yang and E 2000).

### b. Instrumentation

We used two EC systems, a four-component net radiometer, a standard micrometeorological system, and sensors for measuring soil heat flux at this site (Table 2). Both the separated (WindMaster Pro, Gill Instruments Ltd.; and LI-7500A, LI-COR, Inc.) and the integrated (IRGASON) EC systems measured the three-dimensional wind speeds, sonic temperature, and atmospheric $H_2O$ and $CO_2$ concentrations at 10 Hz. Fluxes of momentum, sensible heat ($H$), latent heat ($\lambda E$), and $CO_2$ ($F_c$) were calculated by block averaging from the 10-Hz time series over 30-min intervals. The 30-min average fluxes were recorded by SmartFlux (LI-COR Inc.) and dataloggers (model CR3000, Campbell Scientific, Inc.) for the separated and the integrated EC system, respectively. Coordinate rotation was performed according to the natural wind coordinate system (Lee et al. 2005). Sonic temperature and the sensible

TABLE 2. Summary of the instruments used in this experiment. Term $H$ is sensible heat flux. Term $\lambda E$ is latent heat flux. Term $F_c$ is $CO_2$ flux. Term $u_*$ is friction velocity. Term $\rho_v$ is water vapor density. Terms $u$, $v$, and $w$ are latitudinal, longitudinal, and vertical wind speed, respectively. Term $U$ is mean wind speed. Terms $K_\downarrow$ and $K_\uparrow$ are downward and reflected solar radiation, respectively. Terms $L_\downarrow$ and $L_\uparrow$ are downward and upward longwave radiation, respectively. Term $R_n$ is net radiation. PAR is photosynthesis active radiation. Terms $T_a$ and $T_s$ are air temperature and sonic temperature, respectively. RH is relative humidity.

| Instrument | Sensor | Height/depth (m) | Variables | Operation period |
|---|---|---|---|---|
| EC | LI-7500A (LI-COR, Inc.) + WindMaster Pro (Gill Instruments Ltd.) | 15 | $H$, $\lambda E$, $F_c$, $u_*$, $T_s$, $CO_2$, $\rho_v$, | Jun 2013–10 Mar 2014 |
| | IRGASON (Campbell Scientific, Inc.) | 15 | $u$, $v$, $w$, $U$, wind direction | 16 Dec 2013–3 Jan 2014; 12 Mar 2014–13 Apr 2014 |
| Radiation | CNR4 (Kipp and Zonen B.V.) | 14 | $K_\downarrow$, $K_\uparrow$, $L_\downarrow$, $L_\uparrow$, $R_n$ | Jun 2013–now |
| | PAR LITE (Kipp and Zonen B.V.) | 14 | PAR | Jun 2013–now |
| Micrometeorology | HMP155A (Vaisala Inc.) | 11, 14 | $T_a$, RH | Jun 2013–now |
| | SI-111 (Apogee Instruments, Inc.) | 11 | Surface temperature | Jun 2013–now |
| | TE525MM (Campbell Scientific, Inc.) | 11 | Precipitation | Jun 2013–now |
| Soil | Hukseflux HFP01 (Hukseflux Thermal Sensors B.V.) | 0.08, 0.2, 0.5 | Soil heat flux | Jun 2013–now |

heat flux of both EC systems were corrected for humidity. WPL density corrections were applied to the latent heat flux and the $CO_2$ flux (Webb et al. 1980; Lee and Massman 2011). Correction for angles of attack, which is negligible for CSAT3 anemometers having nearly identical transducer geometry as the IRGASON, was conducted for the Gill sonic anemometer (Nakai et al. 2014). No correction was applied to the Gill/LI-COR system for sensor separation. The meteorological sign convention is used throughout the paper, wherein positive fluxes indicate loss to the atmosphere and negative fluxes indicate uptake by the ecosystem. The suite of auxiliary variables were observed at 1 Hz and also averaged at 30-min intervals.

The field evaluation was conducted during two periods: a winter period from 16 December 2013 to 3 January 2014 and an early spring period from 12 March to 13 April 2014. The LI-7500A analyzer malfunctioned in the spring period, so latent heat flux and $CO_2$ flux were compared only for the winter experiment. Comparison of wind statistics, temperature, and sensible heat flux was based on the data collected in both periods. The chopper motor housing temperature was set to the default (30°C) for LI-7500A to inhibit the accumulation of dew and snow on the IRGA optical window.

### c. Calibration

For the IRGASON, the factory calibration parameters were used. They were checked after the field comparison against a dewpoint generator (model LI-610, LI-COR, Inc.; dewpoint set at 17.00°C) and standard $CO_2$ gas (491.0 ppm, National Institute of Metrology) on 27 May 2014. The dewpoint temperature and $CO_2$ concentration observed by the IRGASON were 16.86°C and 497.4 ppm, respectively. For reference, the slope of the regression of the IRGASON water vapor mixing ratio against the HMP155A water vapor mixing ratio was 0.95 (±0.03) during the same period. The slight discrepancies were within acceptable accuracy thresholds, and no additional post–field correction was made to the IRGASON latent heat flux and $CO_2$ flux.

The LI-7500A analyzer was calibrated in March 2013, and no calibration was performed prior to the comparison experiment. To ensure a valid comparison, we performed a post–field calibration of its water vapor and $CO_2$ measurement against the IRGSASON. A linear regression was performed on the half-hourly water vapor mixing ratio measured by LI-7500A against that measured by IRGASON from 16 to 24 December 2013 and from 25 December 2013 to 3 January 2014, yielding a regression slope of 1.42 (±0.05) and 1.71 (±0.06), respectively. The parameter range of the regression slope represents 95% confidence bounds. The larger-than-unity slope indicates that the LI-7500A's sensitivity was biased high. For post–field calibration, the measured water vapor flux was divided by the slope value to correct the bias error. We performed a linear regression of LI-7500A's half-hourly $CO_2$ mixing ratio against the $CO_2$ mixing ratio measured with the IRGASON, obtaining a slope of 0.82 (±0.03). The $CO_2$ flux measured by LI-7500A was then divided by this slope value.

The post–field calibration is not the best strategy for instrument intercomparison, especially in view of the fact that the calibration resulted in large relative adjustments to the water vapor and $CO_2$ fluxes with the separated EC system. We did the calibration so that we could properly compare the two EC systems, but we acknowledge that our results were not meant to determine which EC system was more accurate. We also note that these post–field adjustments did not compromise our primary

objective—to assess the performance of the IRGASON—and the associated conclusions.

*d. Temperature-related spectroscopic effect*

The $CO_2$ density measured by the IRGASON is proportional to the infrared light absorption $A$ (dimensionless; Jamieson et al. 1963):

$$A = \frac{N}{(\Delta\nu)} \int_{\nu_1}^{\nu_2} \left(1 - \exp\left\{ - \frac{S_i \alpha_i CL}{\pi[(\nu - \nu_{0i})^2 + \alpha_i^2]} \right\}\right) d\nu, \quad (1)$$

where $N$ ($\mu m^{-1}$) is the number of absorption lines in the spectral interval $\Delta\nu$; $\nu_0$ ($\mu m^{-1}$) is the wavenumber of the $i$th spectral line; $C$ (mol $m^{-3}$) is the density of the absorber gas, $L$ (m) is the optical pathlength, $S_i$ (dimensionless) and $\alpha_i$ ($cm^{-1}$) are the strength and Lorentzian half-width of the $i$th individual line, respectively. Both the $S_i$ and $\alpha_i$ are affected by ambient pressure ($P$, Pa) and air temperature ($T$, K), where

$$S_i = f_1(T, P) \quad \alpha_i = f_2(T, P). \quad (2)$$

These dependences are referred to as the spectroscopic effect. The Lorentzian half-width at $T$ and $P$ can be calculated from the Lorentzian half-width under standard atmospheric conditions ($T_0$ = 273 K, $P_0$ = 101 325 Pa)–($\alpha_0$), where

$$\alpha_i(P, T) = \alpha_0 \frac{P}{P_0} \left(\frac{T_0}{T}\right)^{1/2}, \quad (3)$$

Recently, Bogoev et al. (2015) found that the manufacturer's firmware for correcting the spectroscopic effect of the IRGASON's gas analyzer is incomplete. Currently, a standard IRGASON uses air temperature measured with a slow-response sensor to correct for the effect. By switching to the fast-response temperature measured by the sonic anemometer, they were able to remove nearly all of the bias error compared to a closed-path EC system. Their test result yielded the following adjustment equation:

$$F_c' = F_c + 0.014\,257H - 0.066\,828, \quad (4)$$

where $F_c$ and $F_c'$ are the $CO_2$ flux before and after the post–field spectroscopic correction ($\mu mol\ m^{-2}\ s^{-1}$), respectively. The sensible heat flux $H$ is in watts per meters squared. The coefficient of 0.014 257 and −0.066 828 is in $\mu mol\ m^{-2}\ s^{-1}$ per W $m^{-2}$ and $\mu mol\ m^{-2}\ s^{-1}$, respectively.

The theoretical foundation of Eq. (4) can be understood through a linear perturbation analysis in Eq. (1). Let the tilde (˜) denote a quantity obtained with the slow-response temperature measurement. For example, air temperature can be decomposed to $T = \tilde{T} + T'$. Using the Taylor expansion and omitting higher-order terms, we obtain

$$\alpha = \tilde{\alpha} + \Delta\alpha, \quad \tilde{\alpha} = \alpha_o \frac{P}{P_o} \left(\frac{T_o}{\tilde{T}}\right)^{1/2}, \quad \Delta\alpha = -\frac{1}{2}\tilde{\alpha}\frac{T'}{\tilde{T}}. \quad (5)$$

Similarly, the light absorption can be decomposed into the part determined with $\tilde{T}$ and a perturbation part as $A = \tilde{A} + \Delta A$. After some lengthy manipulation involving the Taylor expansion of the function being integrated in Eq. (1), we obtain

$$\Delta A = -\tilde{A}\frac{\Delta\alpha}{\tilde{\alpha}} = \tilde{A}\frac{1}{2}\frac{T'}{\tilde{T}}, \quad A = \tilde{A}\left(1 + \frac{1}{2}\frac{T'}{\tilde{T}}\right). \quad (6)$$

This derivation has used the fact that the exponent in Eq. (1) is much smaller than unity at ambient $CO_2$ levels, and that the perturbation wavenumber $\nu - \nu_o$ is much smaller in magnitude than the Lorentzian half-width. Because the $CO_2$ density $C$ is in proportion to the line absorption, we can write

$$C = \tilde{C}\left(1 + \frac{1}{2}\frac{T'}{\tilde{T}}\right), \quad (7)$$

where $\tilde{C}$ is the default output based on the slow temperature measurement, and $C$ is the signal based on the fast temperature measurement. Multiplying Eq. (7) by the fluctuating vertical velocity and performing Reynolds averaging, we obtain an approximate expression for the relationship between $F_c'$ and $F_c$,

$$F_c' \approx F_c + \frac{1}{2}\frac{1}{\rho c_p}\frac{\overline{C}}{\overline{T}}H, \quad (8)$$

where $\rho$ (kg $m^{-3}$) is air density and $c_p$ (1004 J $kg^{-1}$ $K^{-1}$) is specific heat of air at constant pressure. In typical atmospheric conditions, the parameter group in front of $H$ (W $m^{-2}$) is about 0.025 $\mu mol\ m^{-2}\ s^{-1}$ per W $m^{-2}$, about twice the proportionality coefficient in Eq. (4). The disparity may be contributed by two main factors. First, Eq. (8) has omitted the line strength response to temperature fluctuations, which occurs in the opposite direction to the half-width. As temperature increases, the line width will increase but the line strength will decrease (Bogoev et al. 2015). Second, Eq. (8) assumes that the slow temperature sensor has a time constant comparable to the Reynolds averaging length, but in reality it has a frequency response of 0.01–0.05 Hz. Nevertheless, Eq. (8) confirms that the correction term is indeed proportional to the sensible heat flux. [The intercept coefficient in Eq. (4) is not significantly different from zero.]

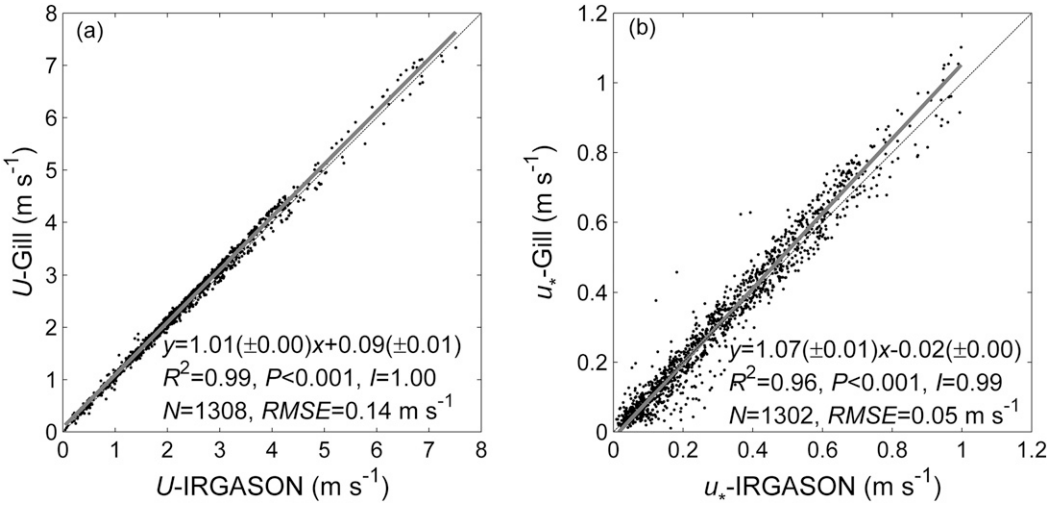


FIG. 2. Comparison between half-hourly (a) wind speed $U$ and (b) friction velocity $u_*$ observed with the Gill sonic anemometer and the IRGASON within the wind direction range of 0°–180° in the compass coordinate system. Solid line represents geometric mean regression with regression statistics noted. The parameter range of the regression statistics represents 95% confidence bounds. The number of observations ($N$), the index of agreement ($I$), and the root-mean-square error (RMSE) are also indicated.

## 3. Results and discussion

### a. Wind statistics

To avoid the effects of flow distortion by the tower structure (Horst et al. 2015, 2016), we restricted the comparison of wind statistics with data collected within the wind direction range of ±90° from the negative $x$ axis of the IRGASON (0°–180° in the compass coordinate system). About 50% of the observations satisfied this wind screening criterion. As shown in Fig. 2, the IRGASON-derived wind speed agreed well with that from the Gill anemometer, showing a difference of less than 1%. The friction velocity from the Gill was 7% higher than the IRGASON value. The difference is within the difference range (3%–15%) of other anemometer intercomparison results (El-Madany et al. 2013) and is about twice the difference between a CSAT3 and a Gill sonic anemometer found by Nakai et al. (2014). The variances of wind speed and friction velocity for the two EC systems are statistically the same at the 1% significance level using the $F$ test. The $t$ test shows that the means of two wind statistics are statistically the same at the 1% significance level.

Flow interference of the triangle-shaped tower (Fig. 1) was a concern to us. The Monin–Obukhov scaling relationships were employed to assess whether the measurements suffered from interference by the instrument structure, its mounting hardware, and the tower. Here we compared the observations within the valid wind direction range (0°–180°) with the established relationship between $\sigma_w/u_*$ and the Monin–Obukhov stability parameter $\zeta$ in the literature (Garratt 1992; Kaimal and Finnigan 1994),

$$\frac{\sigma_w}{u_*} = 1.25(1-3\zeta)^{1/3} \quad \zeta < 0$$

$$\frac{\sigma_w}{u_*} = 1.25(1+0.2\zeta) \quad \zeta > 0, \tag{9}$$

where $\sigma_w$ is the standard deviation of the vertical wind speed, $u_*$ is the friction velocity, and $\zeta$ is the Monin–Obukhov stability parameter. If dynamic flow interference exists, then the observations would deviate from Eq. (9) significantly. Figure 3 shows that the observed pattern of $\sigma_w/u_*$ versus $\zeta$ agreed reasonably well with the relationship described by Eq. (9) for both the separated and integrated EC systems. The neutral $\sigma_w/u_*$ value for the IRGASON (1.19 ± 0.14) and Gill (1.18 ± 0.09) was a little smaller than the standard neutral value of 1.25. The results suggest that the interference of the instrument structure and the tower was negligible in the selected wind direction ranges.

The normalized power spectra of $u$, $v$, and $w$ measured by the Gill and IRGASON followed the −2/3 power law in the inertial subrange (Fig. 4). They all were characterized by a steeper slope in the low- and high-frequency ends than the model spectra proposed by Moore (1986). As compared to the Gill anemometer, lower spectra of $w$ were observed by the IRGASON in the high-frequency range. The normalized $u$–$w$ cospectrum measured by the two sensors obeyed the −4/3 power law in the inertial subrange. The $u$–$w$ cospectrum for

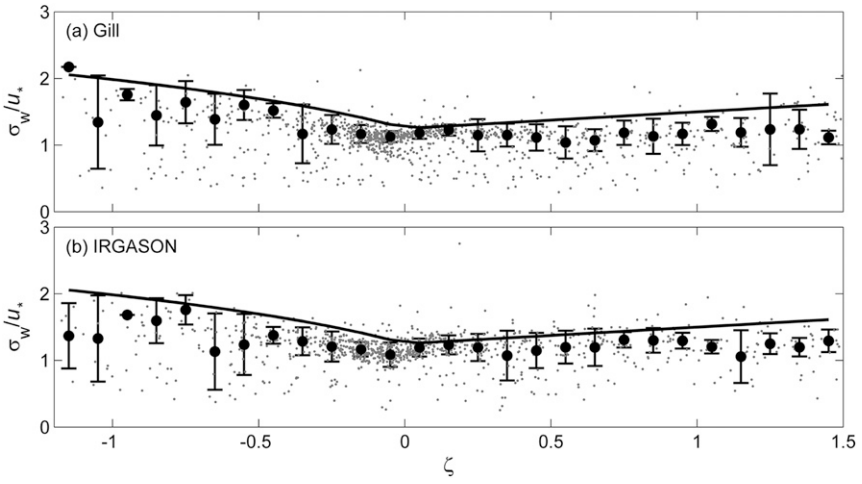


FIG. 3. Variation in $\sigma_w/u_*$ with the Monin–Obukhov stability parameter $\zeta$. Small gray dots denote 30-min observations, and large black dots denote bin-averaged observations (bin width of 0.1). The plot was made for data collected within the wind direction range of 0°–180° in the compass coordinate system. The black lines represent the published relationship between $\sigma_w/u_*$ and $\zeta$ (Garratt 1992; Kaimal and Finnigan 1994). Error bars are one standard deviation of $\sigma_w/u_*$ for each bin.

the two sensors showed more scatter than the wind components' spectra did (Fig. 4).

Ideally, the long-term mean vertical velocity should be zero if the anemometer is aligned with the mean flow streamline over the local terrain (Baldocchi et al. 2000). If the anemometer is tilted slightly, in the absence of flow interference, then the ratio of the half-hourly mean vertical velocity to the horizontal velocity measured in the instrument coordinate should be a sinusoidal function of wind direction. Figure 5 shows that the Gill deviated from the expected behavior in the wind direction range from 210° to 270° because of the shadowing effect of the tower. Outside of the shadowing range, the velocity ratio was persistently positive rather than oscillating around zero on a sinusoidal curve, suggesting a small offset in the measured mean vertical velocity. The tower shadowing effect was less severe on the IRGASON. In the winter experiment, the IRGAON was leveled nearly perfectly, and the half-hourly velocity ratio basically fluctuated around the zero value. In the spring period, it was tilted at about 5°, resulting in a clear sinusoidal dependence on wind direction. There is no evidence of interference from the IRGA's sensing head integrated in the IRGASON. At this site, the majority of observations occurred with wind from the northeast (0°–80°) to northwest (300° –360°). In these quadrants, tower interference was negligible.

### b. *Temperature and sensible heat flux*

Given the arid environment, sonic temperature is expected to be very close to air temperature. The mean water vapor mixing ratio was 2730 ppm in the winter experiment and 3390 ppm in the spring experiment. The IRGASON sonic temperature showed excellent agreement with the air temperature measured with the HMP155A sensor (Fig. 6), with a linear regression slope of 0.98 ± 0.00. The Gill sonic temperature was higher than the air temperature during noontime and lower at midnight in the winter experiment. Using all the data, the linear regression of the Gill temperature against the air temperature resulted in a slope value of 1.09 ± 0.01. A large scatter is evident below the freezing point. Wauben and van Krimpen (2008) also reported large temperature deviations for a Gill WindMaster Pro unit in a climate chamber test. The nonlinear response of Gill sonic temperature to ambient temperature is also documented by Loescher et al. (2005), especially at low operating temperatures (Richiardone et al. 2012).

Figure 7 compares the sensible heat flux measured with the two EC systems. Consistent with the higher sonic temperature sensitivity displayed by the Gill anemometer, the sensible heat flux from the Gill was about 10% higher than that determined by the IRGASON. The mean bias (IRGASON minus Gill) was $-2.8 \pm 18.5\,\mathrm{W\,m^{-2}}$ (mean ± one standard deviation). If we removed the sensitivity difference by dividing the sensible heat flux by the respective slope value of the temperature regression (Fig. 6), then the mean bias was reduced to $0.4 \pm 15.6\,\mathrm{W\,m^{-2}}$. The comparison shown in Fig. 7 was made without wind direction screening. Wind directional screening did not improve the comparison (Fig. S2).

The regression statistics for the sensible heat flux changed only slightly when the data obtained above 0°C

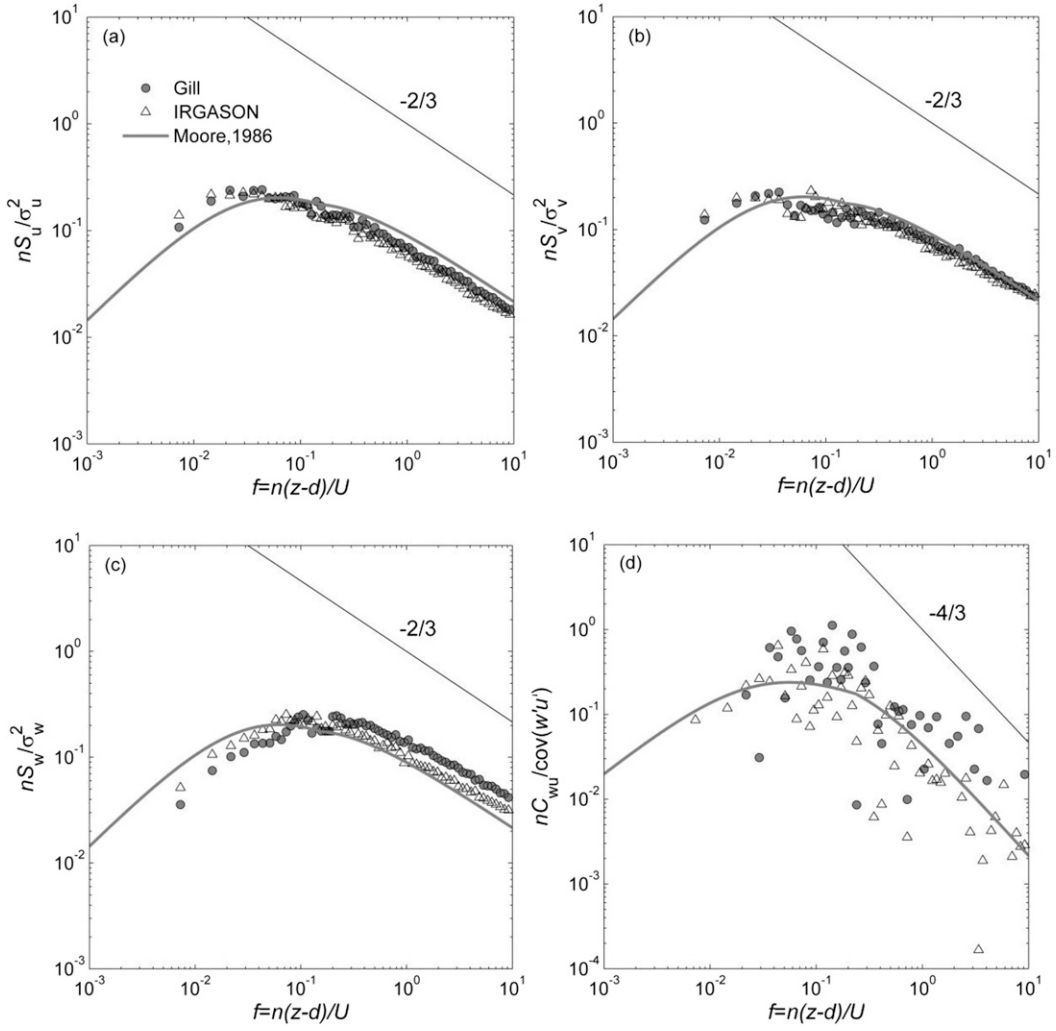


FIG. 4. Ensemble averaged normalized power spectra of (a) the latitudinal wind speed $u$, (b) the longitudinal wind speed $v$, (c) the vertical wind speed $w$, and (d) the $u$–$w$ cospectrum for Gill (solid circle) and IRGASON (hollow triangle). Half-hour data from 1000 to 1300 LT over the winter experiment (from 16 Dec 2013 to 3 Jan 2014) were used. The spectra and cospectrum models of Moore (1986) are shown as the solid gray line. The normalized surface layer frequency $f = n\,(z - d)/U$ is used for the $x$ axis, where $n$ (Hz) is the natural frequency, $z$ (m) is the measurement height, $d$ (m) is the zero-plane displacement, and $U$ (m s$^{-1}$) is the mean wind speed.

air temperature were selected. Even though its performance was poor with regard to the mean temperature measurement, the Gill anemometer/thermometer was able to observe the sensible heat flux reasonably well below the freezing point, in agreement with the study of Loescher et al. (2005).

### c. $CO_2$ flux

Figure 8 shows the time series of the WPL-corrected $CO_2$ flux measured by the IRGASON and the corresponding air temperature. The time series for the separated EC is given in the online supplement (Fig. S3). Valid data were obtained for about 90% of the observations. In the winter period, the IRGASON $CO_2$ flux showed obvious diurnal patterns with apparent sinks during the daytime. The observed $CO_2$ flux varied between $-7$ and $4\,\mu$mol m$^{-2}$ s$^{-1}$. The midday [1100–1300 local time (LT)] mean flux was $-1.65\,\mu$mol m$^{-2}$ s$^{-1}$ (Fig. 9).

Under the arid conditions in the study area, the density effect associated with temperature fluctuations dominated the WPL correction (Fig. 9). For the IRGASON, the temperature WPL correction term was between $-3.57$ and $11.21\,\mu$mol m$^{-2}$ s$^{-1}$, corresponding to a sensible heat flux of $-71.9$ to 230.7 W m$^{-2}$. The water vapor WPL correction term varied from $-0.09$ to $0.28\,\mu$mol m$^{-2}$ s$^{-1}$, corresponding to a latent heat flux variation from $-12.4$ and 36.3 W m$^{-2}$. Correction for ambient pressure fluctuations was negligibly small

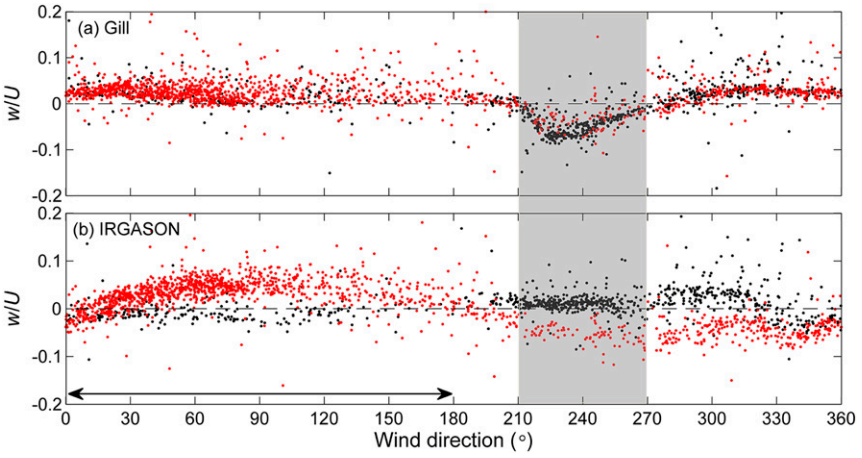


FIG. 5. The relation between the ratio of the half-hourly mean vertical wind speed ($w$) to mean wind speed ($U$) and wind direction. The shaded range indicates wind directions influenced by the tower structure, and double arrows indicate the desirable wind direction range for the IRGASON. Black dots denote winter experiment and red dots denote spring experiment.

($0.007\,\mu\text{mol}\,\text{m}^{-2}\,\text{s}^{-1}$) according to the parameterization proposed by Zhang et al. (2011).

The $CO_2$ flux measured with the separated EC showed similar behaviors to the IRGASON flux (Figs. S3–S5). The $CO_2$ flux comparison between the two systems showed much more relative scatter than did the sensible heat (Fig. 7) and latent heat flux comparison (Fig. S6), which underscores the difficulty in measuring the $CO_2$ flux in the cold desert environment. Uncertainty in the WPL density correction is believed to be a major source of the scatter. A typical measurement noise of $10\,\text{W}\,\text{m}^{-2}$ in the sensible heat flux would cause an error of $0.91\,\mu\text{mol}\,\text{m}^{-2}\,\text{s}^{-1}$ to the temperature WPL correction term, which is about half of the $CO_2$ flux observed at vegetated sites in the off-season (Table 1). The mean difference in the $CO_2$ flux (IRGASON minus separated EC) was $0.03 \pm 1.40\,\mu\text{mol}\,\text{m}^{-2}\,\text{s}^{-1}$ for the whole winter period.

In the early spring period, the IRGASON $CO_2$ flux showed a similar diurnal pattern but with larger midday uptakes than the winter results. The observed $CO_2$ flux varied between $-11.23$ and $4.41\,\mu\text{mol}\,\text{m}^{-2}\,\text{s}^{-1}$. But for day of year (DOY) 78 and DOY 98, the IRGASON observed almost all-day $CO_2$ efflux. The temperature WPL correction term was between $-3.67$ and $19.71\,\mu\text{mol}\,\text{m}^{-2}\,\text{s}^{-1}$, corresponding to the sensible heat flux from $-91.4$ to $496.1\,\text{W}\,\text{m}^{-2}$. The water vapor WPL correction term varied from $-0.14$ to $0.29\,\mu\text{mol}\,\text{m}^{-2}\,\text{s}^{-1}$, corresponding to the latent heat flux variation from $-19.4$ and $35.2\,\text{W}\,\text{m}^{-2}$.

Our winter $CO_2$ fluxes are comparable to those reported in the literature for the off-season or winter periods by open-path EC systems (Table 1). The mean $CO_2$ flux in the winter experiment was $-0.25\,\mu\text{mol}\,\text{m}^{-2}\,\text{s}^{-1}$ ($-0.26\,\text{g}\,\text{C}\,\text{m}^{-2}\,\text{day}^{-1}$) and $-0.22\,\mu\text{mol}\,\text{m}^{-2}\,\text{s}^{-1}$ ($-0.23\,\text{g}\,\text{C}\,\text{m}^{-2}\,\text{day}^{-1}$) for the separated EC system and the IRGASON, respectively. The $CO_2$ flux magnitude observed here was comparable to those reported for the Mojave Desert during winter seasons ($-0.3\,\text{g}\,\text{C}\,\text{m}^{-2}\,\text{day}^{-1}$; Wohlfahrt et al. 2008). The 19-day cumulative carbon flux of the winter experiment was $-4.39$ and $-3.84\,\text{g}\,\text{C}\,\text{m}^{-2}$

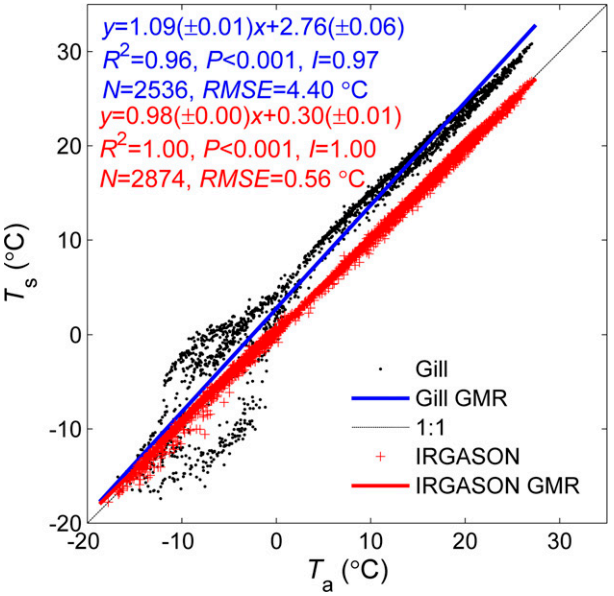


FIG. 6. Relationship between sonic temperature ($T_s$) and air temperature ($T_a$). Solid line represents geometric mean regression (GMR) with regression statistics noted. The parameter range of the regression statistics represents 95% confidence bounds. The number of observations ($N$), the index of agreement ($I$,) and the root-mean-square error (RMSE) are also indicated.

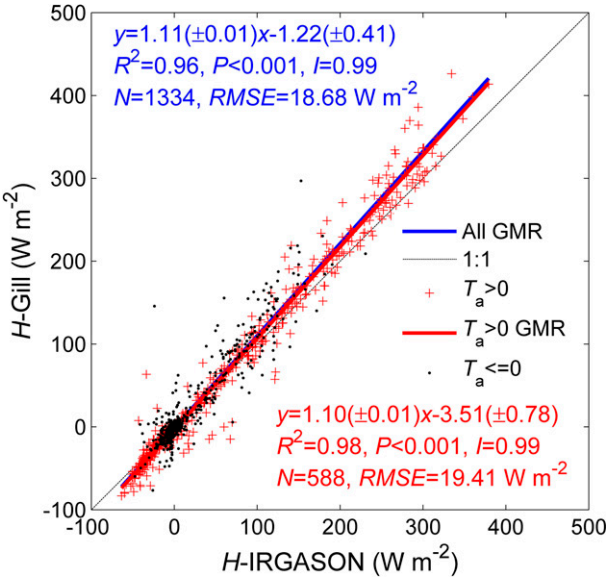


FIG. 7. Relationship between sensible heat flux ($H$) with the Gill and the IRGASON. Solid line represents GMR with regression statistics noted. The parameter range of the regression statistics represents 95% confidence bounds. The number of observations ($N$), the index of agreement ($I$) and the root-mean-square error (RMSE) are also indicated. Regressions were conducted with the whole dataset (blue line) and data above the freezing point (red crosses and red line).

according to the separated EC and the IRGASON, respectively.

### d. Sensor self-heating versus the spectroscopic effect

The observed negative flux in the winter cannot be biological because the trees were dormant without any leaves to support photosynthesis activity. Chemical reactions in arid soils can potentially serve as a sink of atmospheric carbon dioxide (Stone 2008). However, a recent chamber study indicates that the flux associated with soil chemical sinks is on the order of $-0.2\,\mu\text{mol}\,\text{m}^{-2}\,\text{s}^{-1}$ (Ma et al. 2013), which is an order of magnitude too small to explain our midday negative flux. We conclude that the negative $CO_2$ flux was mostly likely a measurement artifact.

We can also rule out sensor self-heating as the cause of the apparent negative $CO_2$ flux. Our reasoning is supported by four lines of evidence. First, because the IRGA and the sonic anemometer/thermometer of the IRGASON sensed the same air volume, any artificial temperature fluctuations should have been detected in situ and corrected by the post–field WPL procedure. Second, self-heating effects should have been more severe on the $CO_2$ flux measured by the separated EC system, and yet the two systems registered nearly identical negative $CO_2$ flux at midday (around $-1.6\,\mu\text{mol}\,\text{m}^{-2}\,\text{s}^{-1}$). Third, an additional artificial heat flux of $31\,\text{W}\,\text{m}^{-2}$ would be needed to correct the midday $CO_2$ flux from $-1.6\,\mu\text{mol}\,\text{m}^{-2}\,\text{s}^{-1}$ to zero value. The artificial heat flux would have been detected by the IRGASON but not by the separated EC system. However, the mean heat flux bias between the two systems ($0.4\,\text{W}\,\text{m}^{-2}$) is too small to accommodate this artificial flux. Fourth, the internal heating of the IRGASON was out of phase with the observed diurnal flux pattern. A small amount of heat (around 1.0 W) was applied at midnight to the IRGA's sensing window to eliminate the possibility of condensation. Heating was triggered when the air temperature fell below −1°C. If the heating were a significant source of temperature fluctuations in the IRGA's optical path, then an artificial negative $CO_2$ flux would have occurred at midnight instead of midday.

After applying the empirical correction for the spectroscopic effect [Eq. (4)], the IRGASON $CO_2$ flux

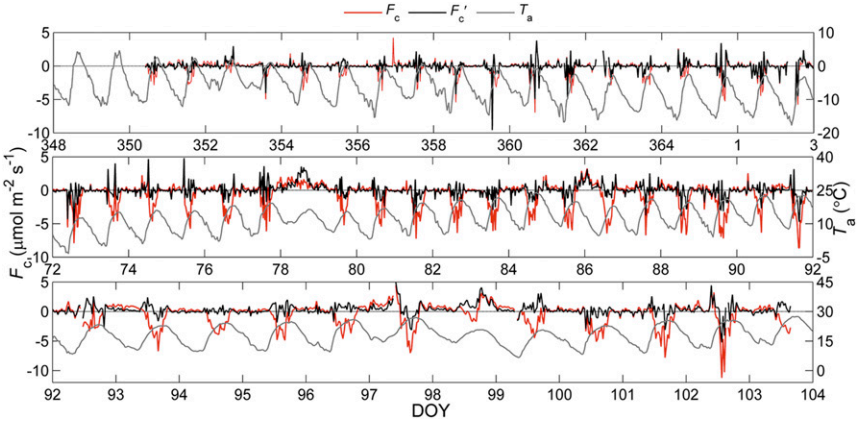


FIG. 8. Time series of the $CO_2$ flux measured with the IRGASON before ($F_c$) and after ($F_c'$) the post–field spectroscopic correction, as well as air temperature ($T_a$) during the two experiments.

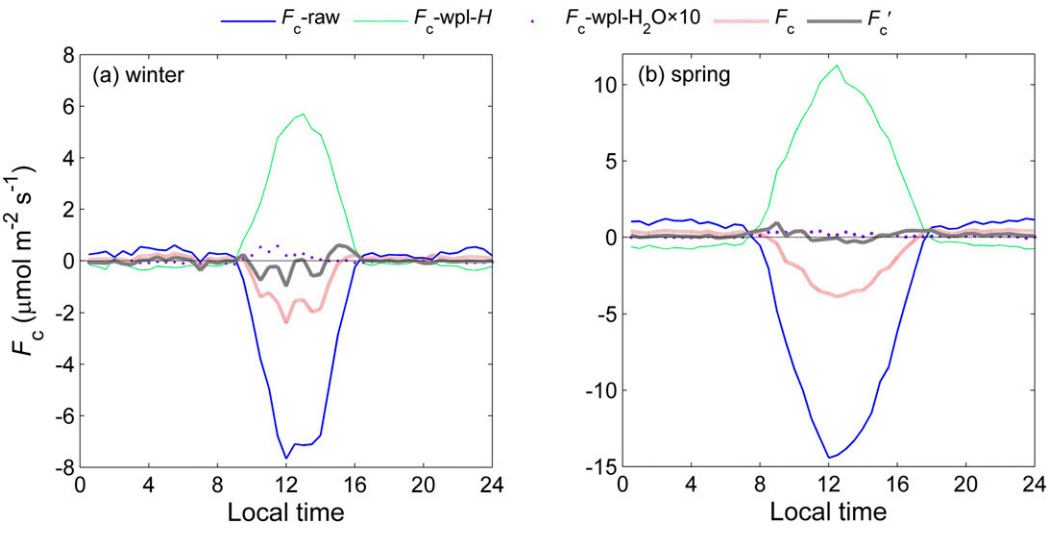


FIG. 9. Diurnal composition of the density correction for $F_c$ averaged over the (a) winter and (b) spring experiments: the raw $CO_2$ flux ($F_c$-raw), temperature WPL correction ($F_c$-wpl-$H$), water vapor WPL correction ($F_c$-wpl-$H_2O$, multiplied by 10), $CO_2$ flux after the WPL density correction ($F_c$), and the $CO_2$ flux after the spectroscopic correction ($F_c'$).

became much closer to zero for both the time series (Fig. 8) and the diurnal composite (Fig. 9) of the winter experiment, resulting in a mean and cumulative $CO_2$ flux of $-0.04\,\mu\text{mol}\,\text{m}^{-2}\,\text{s}^{-1}$ and $-0.77\,\text{g C}\,\text{m}^{-2}$, respectively.

The half-hourly IRGASON $CO_2$ flux after the post–field spectroscopic correction ($-4.93$ to $3.80\,\mu\text{mol}\,\text{m}^{-2}\,\text{s}^{-1}$) was more centralized around zero than that without the correction ($-6.96$ to $4.23\,\mu\text{mol}\,\text{m}^{-2}\,\text{s}^{-1}$). The distribution of the $CO_2$ flux after the spectroscopic correction was a typical normal distribution with 92% observations within the random flux error range ($-1$ to $1\,\mu\text{mol}\,\text{m}^{-2}\,\text{s}^{-1}$) associated with the WPL density correction, which is 6% greater than those without the correction (Fig. 10).

For the spring experiment, the $CO_2$ uptake became much weaker after the spectroscopic correction. With only the WPL correction, the midday IRGASON $CO_2$ flux fluctuated around $-5\,\mu\text{mol}\,\text{m}^{-2}\,\text{s}^{-1}$ (Fig. 9). With the additional spectroscopic correction, the midday IRGASON $CO_2$ flux was near zero at the beginning and became slightly negative at the end of the experiment (Fig. 8). The diurnal composite flux did not show an obvious pattern after the spectroscopic correction. The

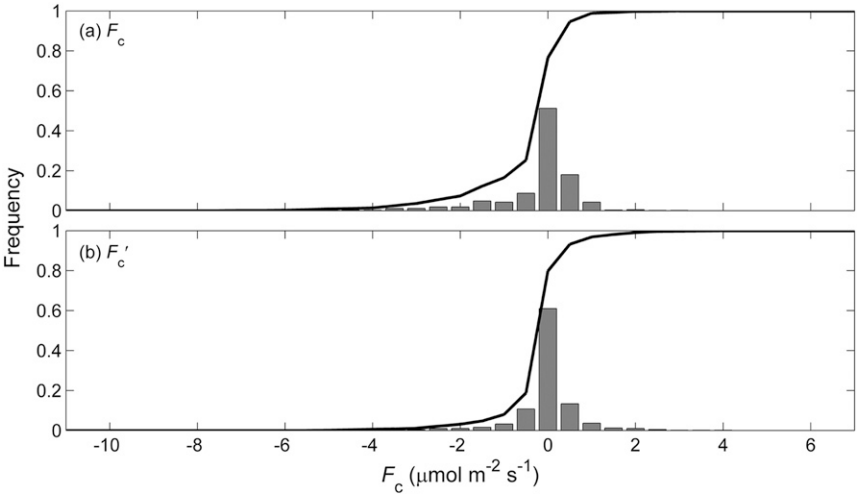


FIG. 10. Frequency distribution of the wintertime IRGASON $CO_2$ flux (a) before ($F_c$) and (b) after ($F_c'$) the spectroscopic correction. The solid lines are the cumulative frequency distribution.

mean $CO_2$ flux was 0.13 and $-0.61\,\mu mol\,m^{-2}\,s^{-1}$ with and without the spectroscopic correction, respectively. Overall, the $CO_2$ flux corrected according to Eq. (4) seems more reasonable for this spare *Populus euphratica* stand at the early flowering stage.

Our results are consistent with that found during an intercomparison between an IRGASON and a closed-path EC conducted in Logan, Utah (Bogoev et al. 2015). The post–field adjustment method for the spectroscopic effect, relating the $CO_2$ flux bias to the sensible heat flux, appears applicable among analyzers from one manufacturer (Helbig et al. 2015), but its generality needs to be further validated across diverse ecosystems, EC setups, and sensor configurations. We caution that the adjustment algorithm as a function of sensible heat flux may have bias and uncertainty associated with the bias and uncertainty of closed-path EC fluxes. Although LI-7500A is not as sensitive to the spectroscopic effect as a laser-based analyzer (e.g., LI-7700, LI-COR Inc.) because of its wide absorption band, the spectroscopic effect correction via manufacturer-determined coefficients may be still inadequate (Edson et al. 2011; Kondo et al. 2014). We speculate that inadequate correction for the spectroscopic effect may partially contribute to artificial $CO_2$ uptake by the open-path EC system, especially in low-$CO_2$ flux conditions.

## 4. Conclusions

We set out to test two hypothesized causes, sensor self-heating and a spectroscopic effect, of negative $CO_2$ fluxes frequently observed in cold seasons when plant photosynthetic uptake is not expected. The IRGASON observed negative $CO_2$ fluxes in the daytime during the winter experiment, with a mean midday flux of $-1.65\,\mu mol\,m^{-2}\,s^{-1}$ despite the fact that the trees were dormant without any sign of photosynthetic activities. Our results support the spectroscopic effect as the more possible cause of the abnormal uptake $CO_2$ flux than sensor self-heating. After applying an additional spectroscopic correction as a function of sensible heat flux, the wintertime IRGASON $CO_2$ flux became physiologically reasonable (mean value of $-0.04\,\mu mol\,m^{-2}\,s^{-1}$).

A simple linear analysis of the line absorption equation deployed by the IRGASON confirms that the post–field spectroscopic correction is proportional to the sensible heat flux. The actual correction formula was established with a different IRGASON unit in a different field experiment (Bogoev et al. 2015). That it was able to remove the negative $CO_2$ flux bias in the present experiment suggests that the coefficient in the empirical formula may be universal for this particular type of gas analyzers.

The above-mentioned conclusions are independent of the comparison of the two systems. A comparison of the IRGASON against the separated EC (Gill and LI-7500A) reveals two additional points. First, the IRGASON showed similar velocity power spectra and cospectrum to the Gill sonic anemometer. And the integral statistics of the two systems agreed reasonably well, and the discrepancy was comparable to those documented in other studies (e.g., Horst et al. 2016). The discrepancy of wind speed was 1% and that of friction velocity was 7%. Second, the separated EC also registered a small midday $CO_2$ flux in the winter ($-1.61\,\mu mol\,m^{-2}\,s^{-1}$). It is not clear whether the same post–field spectroscopic correction should be applied to this type of analyzers.

*Acknowledgments.* This study was supported by the Natural Science Foundation of Jiangsu Province, China (Grant BK20150900), the National Natural Science Foundation of China (Grants 41505005, 41475141, 41275024, and 41271050), the Priority Academic Program Development of Jiangsu Higher Education Institutions (PARD) and the Ministry of Education of China (Grant PCSIRT). The first author acknowledges the support from the Startup Foundation for Introducing Talent of NUIST (Grant 2014r046). We thank Campbell Scientific, Inc. for providing the IRGASON unit, and Xinhua Zhou and Franklin Li for field experiment support and program development.

## REFERENCES

Amiro, B., 2010: Estimating annual carbon dioxide eddy fluxes using open-path analysers for cold forest sites. *Agric. For. Meteor.*, **150**, 1366–1372, doi:10.1016/j.agrformet.2010.06.007.

——, A. Orchansky, and A. Sass, 2006: A perspective on carbon dioxide flux measurements using an open-path infrared gas analyzer in cold environments. *27th Conf. on Agricultural and Forest Meteorology*, San Diego, CA, Amer. Meteor. Soc., P4.7. [Available online at https://ams.confex.com/ams/BLTAgFBioA/techprogram/paper_110015.htm.]

Baldocchi, D., 2014: Measuring fluxes of trace gases and energy between ecosystems and the atmosphere—The state and future of the eddy covariance method. *Global Change Biol.*, **20**, 3600–3609, doi:10.1111/gcb.12649.

——, J. Finnigan, K. Wilson, K. T. Paw U, and E. Falge, 2000: On measuring net ecosystem carbon exchange over tall vegetation on complex terrain. *Bound.-Layer Meteor.*, **96**, 257–291, doi:10.1023/A:1002497616547.

Blanken, P., M. Williams, S. Burns, R. Monson, J. Knowles, K. Chowanski, and T. Ackerman, 2009: A comparison of water and carbon dioxide exchange at a windy alpine tundra and subalpine forest site near Niwot Ridge, Colorado. *Biogeochemistry*, **95**, 61–76, doi:10.1007/s10533-009-9325-9.

Bogoev, I., 2014: Improved eddy flux measurements by open-path gas analyzer and sonic anemometer co-location. *Geophysical Research Abstracts*, Vol. 16, Abstract EGU2014-199. [Available online at http://meetingorganizer.copernicus.org/EGU2014/EGU2014-199.pdf.]

——, M. Helbig, and O. Sonnentag, 2015: On the importance of high-frequency air-temperature fluctuations for spectroscopic corrections of open-path carbon dioxide flux measurement. *Geophysical Research Abstracts*, Vol. 17, Abstract EGU2015-2333. [Available online at http://meetingorganizer.copernicus.org/EGU2015/EGU2015-2333.pdf.]

Bowling, D. R., S. Bethers-Marchetti, C. K. Lunch, E. E. Grote, and J. Belnap, 2010: Carbon, water, and energy fluxes in a semiarid cold desert grassland during and following multiyear drought. *J. Geophys. Res.*, **115**, G04026, doi:10.1029/2010JG001322.

Burba, G. G., D. K. McDermitt, A. Grelle, D. J. Anderson, and L. Xu, 2008: Addressing the influence of instrument surface heat exchange on the measurements of $CO_2$ flux from open-path gas analyzers. *Global Change Biol.*, **14**, 1854–1876, doi:10.1111/j.1365-2486.2008.01606.x.

Cabral, O. M. R., J. H. C. Gash, H. R. Rocha, C. Marsden, M. A. V. Ligo, H. C. Freitas, J. D. Tatsch, and E. Gomes, 2011: Fluxes of $CO_2$ above a plantation of Eucalyptus in southeast Brazil. *Agric. For. Meteor.*, **151**, 49–59, doi:10.1016/j.agrformet.2010.09.003.

Campbell Scientific, Inc., 2016: IRGASON integrated $CO_2$ and $H_2O$ open-path gas analyzer and 3-D sonic anemometer. Instruction Manual, 72 pp.

Chen, Y. N., H. Zilliacus, W. H. Li, H. F. Zhang, and Y. P. Chen, 2006: Ground-water level affects plant species diversity along the lower reaches of the Tarim River, western China. *J. Arid Environ.*, **66**, 231–246, doi:10.1016/j.jaridenv.2005.11.009.

Detto, M., J. Verfaillie, F. Anderson, L. Xu, and D. Baldocchi, 2011: Comparing laser-based open- and closed-path gas analyzers to measure methane fluxes using the eddy covariance method. *Agric. For. Meteor.*, **151**, 1312–1324, doi:10.1016/j.agrformet.2011.05.014.

Edson, J. B., and Coauthors, 2011: Direct covariance measurement of $CO_2$ gas transfer velocity during the 2008 Southern Ocean Gas Exchange Experiment: Wind speed dependency. *J. Geophys. Res.*, **116**, C00F10, doi:10.1029/2011JC007022.

El-Madany, T. S., F. Griessbaum, G. Fratini, J. Y. Juang, S. C. Chang, and O. Klemm, 2013: Comparison of sonic anemometer performance under foggy conditions. *Agric. For. Meteor.*, **173**, 63–73, doi:10.1016/j.agrformet.2013.01.005.

Else, B. G. T., T. N. Papakyriakou, R. J. Galley, W. M. Drennan, L. A. Miller, and H. Thomas, 2011: Wintertime $CO_2$ fluxes in an Arctic polynya using eddy covariance: Evidence for enhanced air-sea gas transfer during ice formation. *J. Geophys. Res.*, **116**, C00G03, doi:10.1029/2010JC006760.

Garratt, J. R., 1992: *The Atmospheric Boundary Layer*. Cambridge Atmospheric and Space Science Series, Cambridge University Press, 316 pp.

Grelle, A., and G. Burba, 2007: Fine-wire thermometer to correct $CO_2$ fluxes by open-path analyzers for artificial density fluctuations. *Agric. For. Meteor.*, **147**, 48–57, doi:10.1016/j.agrformet.2007.06.007.

Ham, J. M., and J. L. Heilman, 2003: Experimental test of density and energy-balance corrections on carbon dioxide flux as measured using open-path eddy covariance. *Agron. J.*, **95**, 1393–1403, doi:10.2134/agronj2003.1393.

Haslwanter, A., A. Hammerle, and G. Wohlfahrt, 2009: Open-path vs. closed-path eddy covariance measurements of the net ecosystem carbon dioxide and water vapour exchange: A long-term perspective. *Agric. For. Meteor.*, **149**, 291–302, doi:10.1016/j.agrformet.2008.08.011.

Helbig, M., E. Humphreys, I. Bogoev, W. L. Quinton, K. Wischnweski, and O. Sonnentag, 2015: Effects of biased $CO_2$ flux measurements by open-path sensors on the interpretation of $CO_2$ flux dynamics at contrasting ecosystems. *Geophysical Research Abstracts*, Vol. 17, Abstract EGU2015-281-1. [Available online at http://meetingorganizer.copernicus.org/EGU2015/EGU2015-281-1.pdf.]

Hirata, R., T. Hirano, N. Saigusa, Y. Fujinuma, K. Inukai, Y. Kitamori, Y. Takahashi, and S. Yamamoto, 2007: Seasonal and interannual variations in carbon dioxide exchange of a temperate larch forest. *Agric. For. Meteor.*, **147**, 110–124, doi:10.1016/j.agrformet.2007.07.005.

Horst, T. W., S. R. Semmer, and G. Maclean, 2015: Correction of a non-orthogonal, three-component sonic anemometer for flow distortion by transducer shadowing. *Bound.-Layer Meteor.*, **155**, 371–395, doi:10.1007/s10546-015-0010-3.

——, R. Vogt, and S. P. Oncley, 2016: Measurements of flow distortion within the IRGASON integrated sonic anemometer and $CO_2$/$H_2O$ gas analyzer. *Bound.-Layer Meteor.*, **160**, 1–15, doi:10.1007/s10546-015-0123-8.

Ikawa, H., and W. C. Oechel, 2015: Temporal variations in air-sea $CO_2$ exchange near large kelp beds near San Diego, California. *J. Geophys. Res. Oceans*, **120**, 50–63, doi:10.1002/2014JC010229.

Jamieson, J. A., R. McFee, G. Plass, R. Grube, and R. Richards, 1963: *Infrared Physics and Engineering*. Inter-University Electronics Series, Vol. 1, McGraw-Hill, 673 pp.

Järvi, L., and Coauthors, 2009: Comparison of net $CO_2$ fluxes measured with open-and closed-path infrared gas analyzers in an urban complex environment. *Boreal Environ. Res.*, **14**, 499–514.

——, A. Nordbo, H. Junninen, A. Riikonen, J. Moilanen, E. Nikinmaa, and T. Vesala, 2012: Seasonal and annual variation of carbon dioxide surface fluxes in Helsinki, Finland, in 2006–2010. *Atmos. Chem. Phys.*, **12**, 8475–8489, doi:10.5194/acp-12-8475-2012.

Kaimal, J. C., and J. J. Finnigan, 1994: *Atmospheric Boundary Layer Flows: Their Structure and Measurement*. Oxford University Press, 289 pp.

Kondo, F., K. Ono, M. Mano, A. Miyata, and O. Tsukamoto, 2014: Experimental evaluation of water vapour cross-sensitivity for accurate eddy covariance measurement of $CO_2$ flux using open-path $CO_2$/$H_2O$ gas analysers. *Tellus*, **66B**, 23803, doi:10.3402/tellusb.v66.23803.

Lafleur, P. M., and E. R. Humphreys, 2008: Spring warming and carbon dioxide exchange over low Arctic tundra in central Canada. *Global Change Biol.*, **14**, 740–756, doi:10.1111/j.1365-2486.2007.01529.x.

Lee, X., and W. Massman, 2011: A perspective on thirty years of the Webb, Pearman and Leuning density corrections. *Bound.-Layer Meteor.*, **139**, 37–59, doi:10.1007/s10546-010-9575-z.

——, K. T. Finnigan, and K. T. Paw U, 2005: Coordinate systems and flux bias error. *Handbook of Micrometeorology: A Guide for Surface Flux Measurement and Analysis*, X. Lee, W. Massman, and B. Law, Eds., Atmospheric and Oceanographic Sciences Library, Vol. 29, Kluwer Academic Publishers, 33–66.

LI-COR, Inc., 2010: LI-7700 open path $CH_4$ gas analyzer instruction manual. 11/2010 980-11617, LI-COR Biosciences, 12 pp. [Available online at https://www.licor.com/env/pdf/gas_analyzers/7700/7700_brochure.pdf.]

Loescher, H. W., and Coauthors, 2005: Comparison of temperature and wind statistics in contrasting environments among different sonic anemometer–thermometers. *Agric. For. Meteor.*, **133**, 119–139, doi:10.1016/j.agrformet.2005.08.009.

Lund, M., and Coauthors, 2015: Low impact of dry conditions on the $CO_2$ exchange of a Northern-Norwegian blanket bog. *Environ. Res. Lett.*, **10**, 025004, doi:10.1088/1748-9326/10/2/025004.

Ma, J., Z.-Y. Wang, B. A. Stevenson, X.-J. Zheng, and Y. Li, 2013: An inorganic $CO_2$ diffusion and dissolution process explains negative $CO_2$ fluxes in saline/alkaline soils. *Sci. Rep.*, **3**, 2025, doi:10.1038/srep02025.

Marcolla, B., and Coauthors, 2011: Climatic controls and ecosystem responses drive the inter-annual variability of the net ecosystem exchange of an alpine meadow. *Agric. For. Meteor.*, **151**, 1233–1243, doi:10.1016/j.agrformet.2011.04.015.

Marushchak, M. E., and Coauthors, 2013: Carbon dioxide balance of subarctic tundra from plot to regional scales. *Biogeosciences*, **10**, 437–452, doi:10.5194/bg-10-437-2013.

McDermitt, D., and Coauthors, 2011: A new low-power, open-path instrument for measuring methane flux by eddy covariance. *Appl. Phys.*, **102B**, 391–405, doi:10.1007/s00340-010-4307-0.

Miller, L. A., and Coauthors, 2011: Carbon dynamics in sea ice: A winter flux time series. *J. Geophys. Res.*, **116**, C02028, doi:10.1029/2011JC007143.

Moore, C. J., 1986: Frequency response corrections for eddy correlation systems. *Bound.-Layer Meteor.*, **37**, 17–35, doi:10.1007/BF00122754.

Nakai, T., H. Iwata, Y. Harazono, and M. Ueyama, 2014: An inter-comparison between Gill and Campbell sonic anemometers. *Agric. For. Meteor.*, **195–196**, 123–131, doi:10.1016/j.agrformet.2014.05.005.

Ono, K., A. Miyata, and T. Yamada, 2008: Apparent downward $CO_2$ flux observed with open-path eddy covariance over a non-vegetated surface. *Theor. Appl. Climatol.*, **92**, 195–208, doi:10.1007/s00704-007-0323-3.

Peel, M. C., B. L. Finlayson, and T. A. McMahon, 2007: Updated world map of the Köppen-Geiger climate classification. *Hydrol. Earth Syst. Sci.*, **11**, 1633–1644, doi:10.5194/hess-11-1633-2007.

Reverter, B. R., E. P. Sánchez-Cañete, V. Resco, P. Serrano-Ortiz, C. Oyonarte, and A. S. Kowalski, 2010: Analyzing the major drivers of NEE in a Mediterranean alpine shrubland. *Biogeosciences*, **7**, 2601–2611, doi:10.5194/bg-7-2601-2010.

——, and Coauthors, 2011: Adjustment of annual NEE and ET for the open-path IRGA self-heating correction: Magnitude and approximation over a range of climate. *Agric. For. Meteor.*, **151**, 1856–1861, doi:10.1016/j.agrformet.2011.06.001.

Richiardone, R., M. Manfrin, S. Ferrarese, C. Francone, V. Fernicola, R. M. Gavioso, and L. Mortarini, 2012: Influence of the sonic anemometer temperature calibration on turbulent heat-flux measurements. *Bound.-Layer Meteor.*, **142**, 425–442, doi:10.1007/s10546-011-9688-z.

Stone, R., 2008: Have Desert Researchers Discovered a Hidden Loop in the Carbon Cycle? *Science*, **320**, 1409–1410, doi:10.1126/science.320.5882.1409.

Wauben, W. M. F., and R. van Krimpen, 2008: Operational test of sonic wind sensors at KNMI. [Available online at http://www.wmo.int/pages/prog/www/IMOP/publications/IOM-96_TECO-2008/P2%2828%29_Wauben_Netherlands.pdf.]

Webb, E. K., G. I. Pearman, and R. Leuning, 1980: Correction of flux measurements for density effects due to heat and water vapour transfer. *Quart. J. Roy. Meteor. Soc.*, **106**, 85–100, doi:10.1002/qj.49710644707.

Welles, J. M., and D. K. McDermitt, 2005: Measuring carbon dioxide in the atmosphere. *Micrometeorology in Agricultural Systems*, J. L. Hatfield, J. M. Baker, and M. K. Viney, Eds., Agronomy Series, Vol. 47, American Society of Agronomy, Inc., Crop Science Society of America, Inc., and Soil Science Society of America, Inc. Publishers, 287–320.

Welp, L. R., J. T. Randerson, and H. P. Liu, 2007: The sensitivity of carbon fluxes to spring warming and summer drought depends on plant functional type in boreal forest ecosystems. *Agric. For. Meteor.*, **147**, 172–185, doi:10.1016/j.agrformet.2007.07.010.

Wohlfahrt, G., L. F. Fenstermaker, and J. A. Arnone III, 2008: Large annual net ecosystem $CO_2$ uptake of a Mojave Desert ecosystem. *Global Change Biol.*, **14**, 1475–1487, doi:10.1111/j.1365-2486.2008.01593.x.

Yang, Z.-H., and Y.-H. E, 2000: A phenology research on the main xylophyte in arid desert area—A example on cultivated plants of Minqin desert botanical garden (in Chinese). *Acta Bot. Boreali-Occident. Sin.*, **6**, 1102–1109.

Yuan, G. F., Y. Luo, M. A. Shao, P. Zhang, and X. C. Zhu, 2015: Evapotranspiration and its main controlling mechanism over the desert riparian forests in the lower Tarim River Basin. *Sci. China Earth Sci.*, **58**, 1032–1042, doi:10.1007/s11430-014-5045-7.

Zhang, J., X. Lee, G. Song, and S. Han, 2011: Pressure correction to the long-term measurement of carbon dioxide flux. *Agric. For. Meteor.*, **151**, 70–77, doi:10.1016/j.agrformet.2010.09.004.